RNA interference knockdown of *DNA methyltransferase 3* affects gene alternative splicing in the honey bee

Hongmei Li-Byarlay[a], Yang Li[b], Hume Stroud[c], Suhua Feng[c], Thomas C. Newman[a], Megan Kaneda[d], Kirk K. Hou[d], Kim C. Worley[e], Christine G. Elsik[f], Samuel A. Wickline[d], Steven E. Jacobsen[c,g,h], Jian Ma[b,i], and Gene E. Robinson[a,i,j,1]

Departments of [a]Entomology and [b]Bioengineering, University of Illinois at Urbana–Champaign, Urbana, IL 61801; [c]Department of Molecular, Cell, and Developmental Biology, University of California, Los Angeles, CA 90095; [d]Department of Computation and Molecular Biophysics, School of Medicine, Washington University, St. Louis, MO 63110; [e]Human Genome Sequencing Center, Baylor College of Medicine, Houston, TX 77030; [f]Divisions of Animal and Plant Sciences, University of Missouri, Columbia, MO 65211; [g]Eli and Edythe Broad Center of Regenerative Medicine and Stem Cell Research and [h]Howard Hughes Medical Institute, University of California, Los Angeles, CA 90095; [i]Institute for Genomic Biology, Urbana, IL 61801; and [j]Neuroscience Program, University of Illinois at Urbana–Champaign, Urbana, IL 61801

Contributed by Gene E. Robinson, June 8, 2013 (sent for review April 10, 2013)

Studies of DNA methylation from fungi, plants, and animals indicate that gene body methylation is ancient and highly conserved in eukaryotic genomes, but its role has not been clearly defined. It has been postulated that regulation of alternative splicing of transcripts was an original function of DNA methylation, but a direct experimental test of the effect of methylation on alternative slicing at the whole genome level has never been performed. To do this, we developed a unique method to administer RNA interference (RNAi) in a high-throughput and noninvasive manner and then used it to knock down the expression of *DNA methyltransferase 3* (*dnmt3*), which is required for de novo DNA methylation. We chose the honey bee (*Apis mellifera*) for this test because it has recently emerged as an important model organism for studying the effects of DNA methylation on development and social behavior, and DNA methylation in honey bees is predominantly on gene bodies. Here we show that *dnmt3* RNAi decreased global genomic methylation level as expected and in addition caused widespread and diverse changes in alternative splicing in fat tissue. Four different types of splicing events were affected by *dnmt3* gene knockdown, and change in two types, exon skipping and intron retention, was directly related to decreased methylation. These results demonstrate that one function of gene body DNA methylation is to regulate alternative splicing.

epigenetics | gene regulation | gene silencing | insect

One of the greatest discoveries of the genomic era is environmental regulation of gene expression; DNA is not just inherited, it is also environmentally responsive. DNA cytosine methylation is an epigenetic mechanism that mediates many environmental influences on gene expression, affecting diverse aspects of organismal function and disease (1), and is one of the best studied mechanisms (2). DNA methylation of CG sites in the promoters of genes in plants and some species of animals acts to repress transcription (3). By contrast, methylation of gene bodies occurs in many species of fungi, plants, and animals (4, 5), but its function has not been clearly elucidated.

We chose to address this issue with the honey bee (*Apis mellifera*) because it has emerged as an important model organism for studying the effects of DNA methylation on development and social behavior (6–9). Moreover, DNA methylation in honey bees is predominantly on gene bodies (7, 8, 10). There are striking differences in methylation between alternative castes that develop from a totipotent female egg—worker and queen (11)—that relate to differences in diet, especially components of royal jelly (12). RNAi silencing of *DNA methyl-transferase 3* (*dnmt3*), which encodes an enzyme involved in de novo methylation (13), alters developmental fate; worker larvae treated with *dnmt3* RNAi show an increased likelihood of developing into queens (11).

Recent studies in both invertebrates and mammals support the idea that methylation is correlated with alternative splicing (AS) of transcripts (7, 14). By comparing brain methylomes of queen and worker bees, a correlation was revealed between DNA methylation and AS (7, 8). An in vitro study of mammalian cells showed that DNA methylation inhibited the binding of transcription factor CCCTC binding factor (CTCF), which affected alternative splicing (14). Regulation of AS is a complicated process that also involves spliceosome assembly (7, 15), chromatin structure (16, 17), siRNA activity (18), and transcriptional elongation (19), in addition to the apparent action of methylation.

To explore the causal relationship of DNA methylation and AS in vivo, we used the honey bee to test for a direct link between DNA methylation and AS. We decreased DNA methylation by *dnmt3* RNA interference (RNAi) and hypothesized that there would be effects on AS.

RNAi has previously been administered to honey bees and other insects for gene knockdown (KD) by injection (20, 21), but this method is time consuming and highly invasive. We developed a unique method to treat large numbers of insects quickly and noninvasively. We coupled small interfering RNA (siRNA) to perfluocarbon-nanoparticles (PFC-NPs) and nebulized the mixture for aerosol application. PFC-NPs have been used in a variety of biomedical applications, including delivery of RNAi to tumor cells (22, 23), but had never before been nebulized.

To test the hypothesis that DNA methylation regulates AS, we used our method to knock down *dnmt3* in honey bee abdominal fat tissue. We chose this tissue because abdominal injections of RNAi have proven especially effective (20, 21), and there are extensive gene expression data from honey bee fat body to compare our results to. Insect fat tissue has analogous functions to both liver and adipose tissue in mammals because they are crucial for both carbohydrate metabolism and lipid storage. We used RNAseq and new AS quantification software (24) to evaluate our hypothesis.

Author contributions: H.L.-B., S.A.W., S.E.J., J.M., and G.E.R. designed research; H.L.-B., Y.L., and T.C.N. performed research; S.F., M.K., K.K.H., K.C.W., and C.G.E. contributed new reagents/analytic tools; H.L.-B., Y.L., H.S., and J.M. analyzed data; and H.L.-B. and G.E.R. wrote the paper.

The authors declare no conflict of interest.

Freely available online through the PNAS open access option.

Data deposition: The sequence reported in this paper has been deposited in the National Center for Biotechnology Information Sequence Read Archive database (accession no. SRP024289).

[1]To whom correspondence should be addressed. E-mail: generobi@illinois.edu.

This article contains supporting information online at www.pnas.org/lookup/suppl/doi:10.1073/pnas.1310735110/-/DCSupplemental.

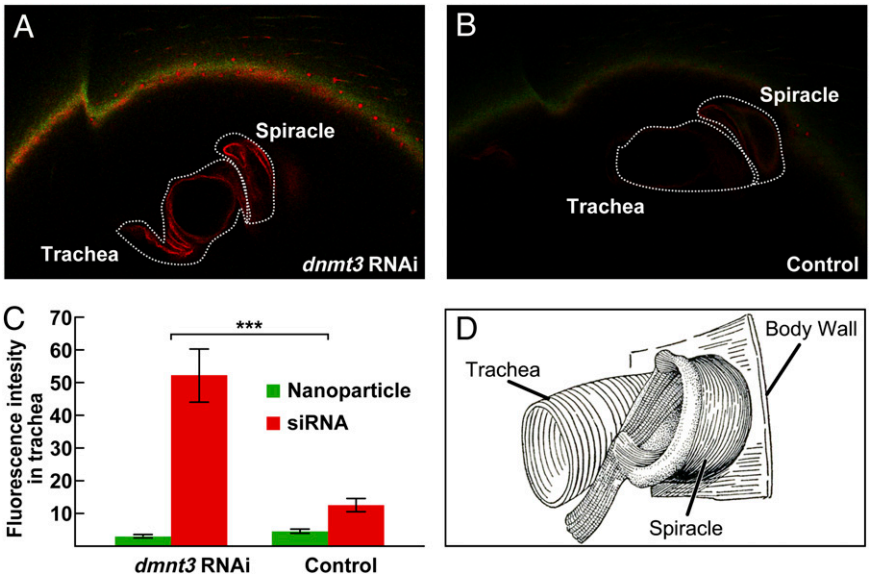

Fig. 1. Noninvasive high-throughput method of delivering RNA interference in vivo. Spraying a nebulized mixture of nanoparticles (PFC-NP) and small interfering RNA (siRNA) on bees allows penetration through the insect tracheal respiratory system. (*A*) Treated: NP (labeled green with Alexa 488) and *dnmt3* siRNA (labeled red with Q-670). (*B*) Control: NP (green) and GFP siRNA (no label). (*C*) Quantitative analysis of fluorescence reveals significantly higher levels of red signal in treated ($n = 5$) comparing to control bees ($n = 6$, $P < 0.001$, two-tailed t test), demonstrating penetration via the trachea. (*D*) Schematic of an inner view of trachea, spiracle atrium, and body wall. Diagram adapted from ref. 25.

Results and Discussion

We first tested the efficacy of our method of administering RNAi. Image analysis indicates that the nebulized nanoparticle–siRNA complex penetrates the spiracles on the thorax and abdomen and travels through the tracheal respiratory system, which functions in insects to deliver oxygen directly to cells via ever-finer branches ending in tracheoles (25). This was shown by spraying caged bees (n = 17–18 bees/cage) with a mixture of PFC-NPs (labeled Alexa 488 in green) and *dnmt3* siRNA (labeled Q-670 in red); control bees were sprayed with PFC-NPs (same label in green) and exogenous GFP siRNA (no label). Confocal microscopy revealed that trachea of *dnmt3* siRNA-treated bees showed significantly higher levels of red fluorescence compared with nonlabeled control bees (Fig. 1). Using the same *dnmt3* RNAi construct (Fig. S1) used previously for a prior honey bee RNAi injection study (11), aerosol application caused an ∼30% knockdown in fat tissue (n = 44 and 42 control and RNAi bees, respectively, across three biological replicates; Fig. 2). We obtained a similar KD by abdominal injection of the PFC-NP–siRNA complex (Fig. S2). By contrast to these results for the abdomen, no consistent KD was detected in the head, so brain analysis was not pursued. This result was unfortunate but not unexpected, given that the penetration points (spiracles) are located on the thorax and abdomen and not the head (25). These results demonstrate that it is possible to effectively exploit the insect tracheal system to deliver siRNA at least to abdominal cells via nebulizing spray in a rapid and noninvasive manner.

dnmt3 siRNA-treated and control bees were used for genome-wide analysis of gene expression, AS, and DNA methylation. We used the TrueSight program to analyze the RNA sequencing

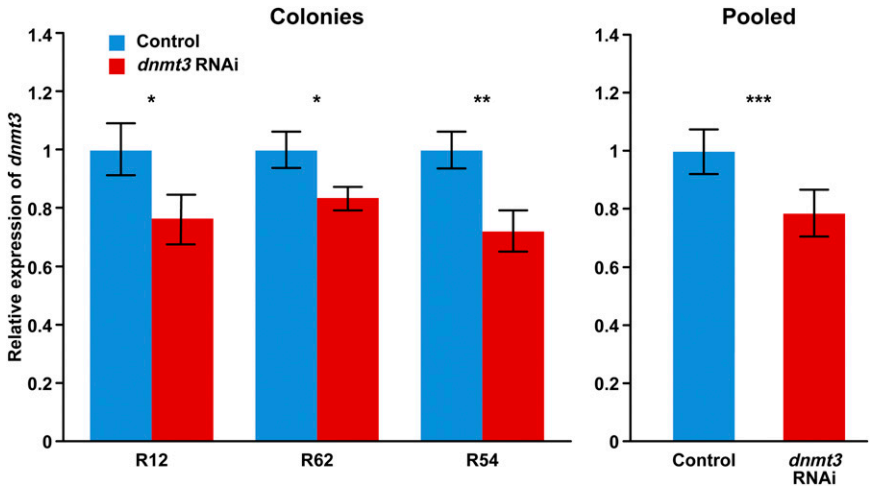

Fig. 2. Effects of spraying a nebulized mixture of nanoparticles and small interfering RNA of *dnmt3* on *dnmt3* expression ± SEM in honey bee abdominal fat body. Results from three biological replicates (bees from unrelated colonies, n = 22 for colony R12; n = 31 for R62, and n = 33 for R54; two-tailed t tests). Analysis of pooled data: mixed-model ANOVA, df = 82, $F = 15.52$. *$P < 0.05$, **$P < 0.01$, ***$P < 0.001$.

Table 1. Effects of *dnmt3* knockdown on DSGs, including types of ES, IR, ATE, and AEB on gene alternative splicing (AS)

Types of AS event	No. of DSGs	FDR	Gene example	*P* value of qPCR validation
ES	192	0.01	*GB53079*	0.002
IR	27	0.1	*GB49485*	0.03
ATE	141	0.01	*GB49165*	0.003
AEB	225	0.01	*GB50039*	0.004

Examples are shown in detail in Fig. 3. AEB, alternative exon boundary; ATE, alternative terminal exon; ES, exon skipping; FDR, false discovery rate; IR, intron retention. Gene examples are shown in detail in Fig. 3.

(RNA-seq) data and quantify AS. Detailed description of this application is in ref. 24. Across treated and control samples, RNA-seq yielded robust expression results for 13,008 genes, estimated to comprise 84.9% of the genes predicted from Assembly 4.5 and Official Gene Set 3.2 of the honey bee genome (http://hymenopteragenome.org/beebase/?q=gbrowse_amel). KD of *dnmt3* caused strong effects on gene expression. A total of 2,613 (17.1%) genes showed significant differential expression due to RNAi treatment. Gene Ontology analysis of a subset of these differentially expressed genes (DEGs) that had orthologs in the *Drosophila melanogaster* genome (2,121) revealed that *dnmt3* KD had particularly strong effects on RNA processing, intracellular transport, and protein catabolic processing (Table S1). Approximately 60.3% of the genes were found to be alternatively spliced, which is consistent with findings from *Drosophila* (26), and lower than in mammals (27, 28).

Comparing our results to previous gene expression studies of fat body, our DEG list also was enriched for genes related to honey bee behavioral maturation, which involves a shift from working in the hive when young to foraging when older (29). We compared our DEG list with DEG lists from fat tissue associated with (*i*) hive vs. forager bees; (*ii*) exposure to poor vs. rich diet

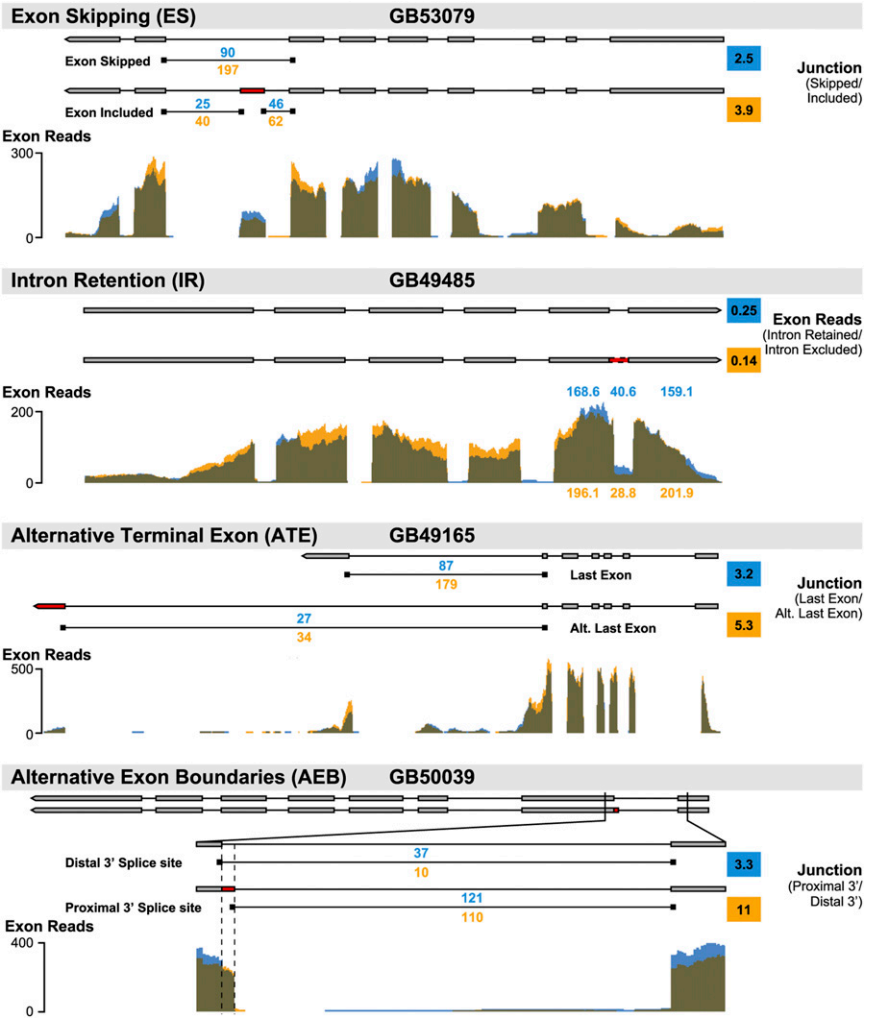

Fig. 3. Effects of *dnmt3* knockdown on differentially spliced genes. (*Upper*) Gene model in both splicing isoforms with the number of RNAseq reads mapped to each splicing junction. (*Lower*) Exon coverage from RNAseq. Blue, control; orange, *dnmt3* knockdown. Derivation of the AS ratios in the colored squares are in *SI Materials and Methods*.

Table 2. Effects of *dnmt3* knockdown (KD) on DNA methylation of DESs and DIRs

Splicing type	Direction	More methylated by *dnmt3* KD	Less methylated by *dnmt3* KD	*P* value
DES	More skipped	13	35	0.019
	Less skipped	14	10	
DIR	Less retained	3	9	0.044
	More retained	3	0	

DES, differentially exon skipped gene; DIR, differentially intron retained gene.

(poor diet accelerates behavioral maturation); and (*iii*) exposure to queen pheromone (which delays behavioral maturation). There were significant overlaps between the *dnmt3* KD DEG list and all three of these DEG lists [298, 368, and 363 genes, respectively; representation factor (RF) = 1.02, 1.37, and 1.37; P = 0.026, 2.36e−12, and 4.34e−12]. There also was a significant overlap of our *dnmt3* KD DEG list and the DEG list from the caste determination study that used *dnmt3*-silenced larvae (11) (RF = 2.62, P = 5.77e−5). These results suggest that nutritional regulation of behavioral maturation involves differential methylation of genes in the honey bee fat body.

KD of *dnmt3* caused strong effects on AS. A total of 524 genes showed significant differences in AS due to treatment [false discovery rate (FDR) < 0.1]. Moreover, there were significant differences for four different types of AS events: exon skipping (ES), alternative terminal exons (ATE), alternative exon boundaries (AEB), and intron retention (IR) (Table 1). This result revealed a broader effect of *dnmt3* KD on AS than expected. Results with quantitative PCR (qPCR) for selected genes (Fig. 3; Fig. S3) confirmed the effects of *dnmt3* KD on AS.

To examine the possibility that *dnmt3* KD exerted its effects by altering the expression of genes known to act as AS factors, we investigated the RNA-seq results for all known AS factors or AS factor-like genes in honey bees (by orthology to *Drosophila*). Of 72 AS factor or AS factor-like genes, 16 were differentially expressed (Table S2). There was no correlation between DNA methylation changes in gene bodies or promoter regions and the expression of these 16 genes (r = 0.25 and −0.12, P = 0.35 and 0.66, respectively). We cannot rule out the possibility that changes in expression of AS factor genes caused all of the above-reported change in AS, but we consider this unlikely, given the close association between the RNAi KD–induced changes in methylation and AS that we detected, as we report in the following paragraphs.

To address the issue of whether the effects of *dnmt3* KD on AS were due to decreases in DNA methylation, *dnmt3* siRNA-treated and control bees were used for genome-wide analysis of DNA methylation by bisulfite sequencing (BS-seq). Using pooled samples for a single analysis of treated and control bees, *dnmt3* KD caused a 21% decrease in DNA methylation, similar to the level of KD of *dnmt3* itself (~30%). Sequencing coverage was comprehensive, covering 86.5% of all cytosine-phosphate-guanines (CpGs) with at least one read in the control and 80.1% in the *dnmt3* KD sample (Fig. S4).

BS-seq results support the contention that the effects of *dnmt3* KD on AS are at least partly due to decreases in DNA methylation. There was a significant relationship between *dnmt3* KD, DNA methylation, and exon skipping: decreased DNA methylation (due to *dnmt3* KD) was associated with increased ES (Table 2; P = 0.019, two-tailed Fisher's exact test, n = 72 differential exon skipping events; Fig. 4). A galactokinase-like gene *GB46657* is represented in Fig. 4 as an example of DNA methylation affecting ES. These genome-wide findings are consistent with results from honey bees for a single gene (8). A study in human cell lines (14) reported that DNA methylation prevented CTCF from binding to the alternative exon, leading to an increase in ES. The specific effect of DNA methylation on AS may vary in different genomic landscapes and in different species (30). Our results provide experimental evidence at the whole-genome level for a direct link between alternative splicing and DNA methylation in a *dnmt3* KD background.

BS-seq also revealed a significant association with decreased DNA methylation and less IR (P = 0.044, two-tailed Fisher's exact test; Table 2). We did not test for a relationship between DNA methylation levels and AEB or ATE because no practical method has been developed yet: alternative exon boundaries are very short in cases of AEB, and ATE is often close to the regulatory regions. Other mechanisms in addition to DNA methylation are thus likely involved in the regulation of different forms of AS. Our results with BS-seq data demonstrate that DNA methylation of gene bodies affects alternative splicing on a genome-wide scale, specifically for ES and IR.

Alternative splicing of mRNA transcripts is an important mechanism for increasing the diversity and complexity of phenotypes that are generated from a genome (31) and can show

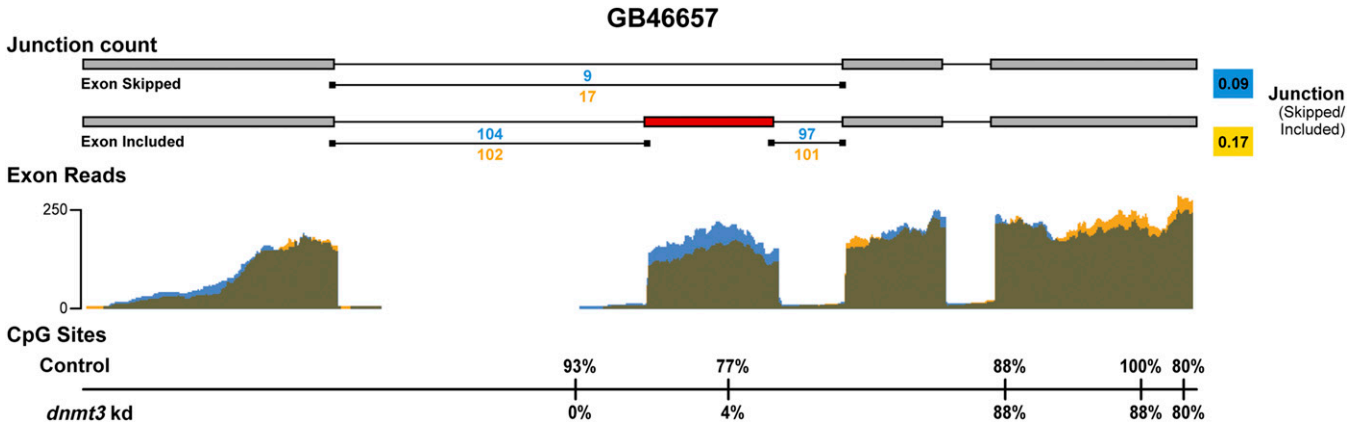

Fig. 4. Effects of *dnmt3* knockdown on exon skipping and methylation in gene GB46657 (galactokinase-like). (*Top* and *Middle*) Same information as in Fig. 3. (*Bottom*) mCpG sites with vertical lines, together with percent differences between treatments.

strong species-specific differences (32, 33). AS has been shown to play fundamental roles in sex determination, development, behavior, and disease, and in worker honey bees, sterility, which is a hallmark of eusociality (1, 34, 35). Recently, DNA methylation has been detected in the genomes of other important social insects including several ants and termites (36, 37) and has been implicated in caste differentiation and behavioral maturation (8, 38). Further studies of DNA methylation and AS will help understand the mechanisms and evolution of phenotypic plasticity.

Materials and Methods

Bees. Honey bees were a mix of European races typical of Illinois, predominantly *Apis mellifera ligustica*. They were maintained according to standard practices at the University of Illinois Bee Research Facility. We used worker bees derived from single-drone inseminated queens for RNA-seq analysis to reduce interindividual genetic variability and worker bees from a naturally mated queen colony for BS-seq analysis. Treated and control bees for each biological replicate were from the same colony.

RNA Interference Treatment. We administered a nebulized aerosol mixture of PFC-NPs made in the Wickline laboratory and small siRNA for *dnmt3* (Sigma). The control was siRNA for EGFP-S1 (IDT). siRNA oligo sequences are given in Table S3. The doses of PFC-NP and siRNA were 200 pM and 1 μM, respectively, in a total volume of 1,368 μL (mixture of PFC-NP, siRNA, and molecular graded water). A higher ratio of *dnmt3* siRNA/NP (200 pM/2 μM) also was tested, but did not appear as efficacious. The reason may be that the number of siRNA molecules per nanoparticle was increased at a higher dose and the charge of the transfection complex changed, so the delivery of the transfection complex was not efficient. This treatment was administered to groups of 17–18 bees for 5 min. After treatment, the bees were placed in a standard Plexiglas cage and held in a dark incubator at 32 °C, 40% relative humidity, for 96 h. They were fed pollen paste [50% (wt/vol) honey/50% (wt/vol) pollen] and sugar syrup [50% sucrose (wt/vol) in water], which was replaced daily. Bees were collected 96 h after spray and frozen in liquid nitrogen, and then kept at −80 °C for analysis. Abdominal fat bodies were stored in RNAlater-ICE (catalog no. AM7030; Ambion by Life Technologies) overnight and then dissected and stored at −80 °C. For injection experiments, PFC-NP:siRNA (10 pM:10 nM) was administered in 400 nL of insect saline solution and administered to 1-d-old bees abdominally. Holding conditions were as for the sprayed bees.

Image Processing to Determine Mode of Action of Nanoparticle–RNAi Spray. To determine whether the nanoparticle-RNAi spray acts by penetrating the insect tracheal respiratory system, 1-d-old bees ($n = 17–18$) were sprayed with both 1 μM siRNA of GFP control (no labeling) and 200 pM Alexa 488 fluorescently labeled nanoparticles (green) or with 1 μM Q-670 siRNA of *dnmt3* (red) and nanoparticles (green) with the above dose. Abdominal spiracles and trachea were dissected in insect saline solution 24 h after spraying. Samples were dehydrated in solutions of 25%, 50%, 75%, 100%, and 100% methanol for 20 min, respectively, and maintained in 100% methyl salicylate until imaging. The images were captured by a Zeiss LSM 700 confocal microscope at 20×.

RNA-seq. We selected individuals showing typical KD for RNA sequencing (6 treated and 6 control). Libraries were made with the TruSeq RNA sample preparation kit per the manufacturer's instructions (Illumina). One library was made per individual and barcoded. The 12 libraries were pooled and quantitated by qPCR, and the pool was sequenced on two lanes for 100 cycles, in paired-end mode, on an Illumina HiSeq2000 machine (Illumina). We used the TruSeq SBS sequencing kit (version 3) and analyzed the results with Casava1.8 (pipeline 1.9). Library construction and RNA-seq sequencing were performed at the University of Illinois W.M. Keck Center for Comparative and Functional Genomics. The number of sequencing reads was ∼56–72 M/sample, and the average cDNA length was 220 bp. Reads from each sample were aligned onto the *A. mellifera* genome assembly v4.5 using TrueSight (24), allowing up to two mismatches for both exonic and junction spanning reads. These reads were mapped to 14,124 genes of 15,314 annotated genes in the Official Gene Set v3.2. TrueSight assigns a probability score to each of the predicted splice junctions for each gene, which indicates their reliability based on coding potentials and RNA-seq mapping quality. We used all splice junctions with TrueSight score greater than 0.5 (on a scale from 0 to 1). BEDTools (39) was used to calculate the read coverage of the nonredundant exon models based on TrueSight mapping results (in binary alignment/map format). Complete methods and further analyses are provided in *SI Materials and Methods*.

BS-seq Analysis. Genomic DNA (1 μg/group) extracted from pooled abdominal fat body samples (18 bees per group) was used to generate BS-seq libraries using the premethylated adapter method based on a previously published protocol (40). The single-end libraries were sequenced on an Illumina HiSeq2000, following the manufacturer's manual. Data processing, aligning Bisulfite-converted reads, and methylation assessments are described in ref. 40. Identical reads were collapsed into single reads. The methylation level was calculated as the ratio of methylated reads over all reads covering each CpG site, using a threshold of 20% methylation and read coverage ≥4 in either control or treated samples. We used this threshold because it resulted in a comparable number of methylated cytosine-phosphate-guanine (mCpG) sites (123,023) to previous studies (7). At this threshold there was no methylated cytosine signal from the mitochondrial genome. *Dnmt3* KD caused an overall decrease in CpG methylation levels (an average of −0.045 per mCpG).

ACKNOWLEDGMENTS. We thank C. Nye for bee colony assistance; A. Duque and D. Dalpiaz for technical assistance in the laboratory; A. Hernandez and the W. M. Keck Center for Comparative and Functional Genomics for library preparation and RNAseq; M. Akhavan for technical assistance; the UCLA BSCRC BioSequencing Core Facility for BS-Seq; Y. Liu for advice on DEG analysis; D. M. Muzny and C. L. Kovar and the BCM-HGSC genome sequencing and assembly teams for the improved *Apis mellifera* genome assembly; A. Bennett, K. Hoff, F. Camara, R. Guigo, T. Murphy, K. Pruitt, V. Soloveyev, and M. Stanke for preparing the Official Gene Set v3.2; and P. L. Jones, R. Maleszka, and members of the G.E.R. laboratory for comments that improved the manuscript. This project was supported by National Institutes of Health (NIH) Director's Pioneer Award 1DP1OD006416 (to G.E.R.), National Science Foundation Grant 1054309 (to J.M.), NIH Grant 1R21HG006464 (to J.M.), NIH Grant R01 HL073646 (to S.A.W.), NIH Grant GM60398 (to S.E.J.), an American Association of University Women American postdoctoral fellowship (to H.L.-B.), and an American Heart Association Heartland Affiliate predoctoral training grant (to M.K.). S.F. is a Special Fellow of the Leukemia and Lymphoma Society. S.E.J. is an Investigator of the Howard Hughes Medical Institute.

1. Edwards TM, Myers JP (2007) Environmental exposures and gene regulation in disease etiology. *Environ Health Perspect* 115(9):1264–1270.
2. Suzuki MM, Bird A (2008) DNA methylation landscapes: Provocative insights from epigenomics. *Nat Rev Genet* 9(6):465–476.
3. Law JA, Jacobsen SE (2010) Establishing, maintaining and modifying DNA methylation patterns in plants and animals. *Nat Rev Genet* 11(3):204–220.
4. Zemach A, McDaniel IE, Silva P, Zilberman D (2010) Genome-wide evolutionary analysis of eukaryotic DNA methylation. *Science* 328(5980):916–919.
5. Jones PA (2012) Functions of DNA methylation: Islands, start sites, gene bodies and beyond. *Nat Rev Genet* 13(7):484–492.
6. Wang Y, et al. (2006) Functional CpG methylation system in a social insect. *Science* 314(5799):645–647.
7. Foret S, et al. (2012) DNA methylation dynamics, metabolic fluxes, gene splicing, and alternative phenotypes in honey bees. *Proc Natl Acad Sci USA* 109(13):4968–4973.
8. Lyko F, et al. (2010) The honey bee epigenomes: Differential methylation of brain DNA in queens and workers. *PLoS Biol* 8(11):e1000506.
9. Lyko F, Maleszka R (2011) Insects as innovative models for functional studies of DNA methylation. *Trends Genet* 27(4):127–131.
10. Consortium HGS; Honeybee Genome Sequencing Consortium (2006) Insights into social insects from the genome of the honeybee Apis mellifera. *Nature* 443(7114): 931–949.
11. Kucharski R, Maleszka J, Foret S, Maleszka R (2008) Nutritional control of reproductive status in honeybees via DNA methylation. *Science* 319(5871): 1827–1830.
12. Kamakura M (2011) Royalactin induces queen differentiation in honeybees. *Nature* 473(7348):478–483.
13. Goll MG, Bestor TH (2005) Eukaryotic cytosine methyltransferases. *Annu Rev Biochem* 74:481–514.
14. Shukla S, et al. (2011) CTCF-promoted RNA polymerase II pausing links DNA methylation to splicing. *Nature* 479(7371):74–79.
15. Black DL (2003) Mechanisms of alternative pre-messenger RNA splicing. *Annu Rev Biochem* 72:291–336.
16. Schor IE, Rascovan N, Pelisch F, Alló M, Kornblihtt AR (2009) Neuronal cell depolarization induces intragenic chromatin modifications affecting NCAM alternative splicing. *Proc Natl Acad Sci USA* 106(11):4325–4330.
17. Hnilicová J, et al. (2011) Histone deacetylase activity modulates alternative splicing. *PLoS ONE* 6(2):e16727.

18. Kim DH, Villeneuve LM, Morris KV, Rossi JJ (2006) Argonaute-1 directs siRNA-mediated transcriptional gene silencing in human cells. *Nat Struct Mol Biol* 13(9): 793–797.
19. Selth LA, Sigurdsson S, Svejstrup JQ (2010) Transcript elongation by RNA polymerase II. *Annu Rev Biochem* 79:271–293.
20. Nelson CM, Ihle KE, Fondrk MK, Page RE, Amdam GV (2007) The gene vitellogenin has multiple coordinating effects on social organization. *PLoS Biol* 5(3):e62.
21. Ament SA, et al. (2012) The transcription factor ultraspiracle influences honey bee social behavior and behavior-related gene expression. *PLoS Genet* 8(3): e1002596.
22. Kaneda MM, Sasaki Y, Lanza GM, Milbrandt J, Wickline SA (2010) Mechanisms of nucleotide trafficking during siRNA delivery to endothelial cells using perfluorocarbon nanoemulsions. *Biomaterials* 31(11):3079–3086.
23. Soman NR, et al. (2009) Molecularly targeted nanocarriers deliver the cytolytic peptide melittin specifically to tumor cells in mice, reducing tumor growth. *J Clin Invest* 119(9):2830–2842.
24. Li Y, et al. (2013) TrueSight: A new algorithm for splice junction detection using RNA-seq. *Nucleic Acids Res* 41(4):e51.
25. Snodgrass RE (1956) *Anatomy of the Honey Bee* (Comstock Publishing Associates, New York), pp 230–240.
26. Graveley BR, et al. (2011) The developmental transcriptome of *Drosophila melanogaster*. *Nature* 471(7339):473–479.
27. Pan Q, Shai O, Lee LJ, Frey BJ, Blencowe BJ (2008) Deep surveying of alternative splicing complexity in the human transcriptome by high-throughput sequencing. *Nat Genet* 40(12):1413–1415.
28. Wang Z, Burge CB (2008) Splicing regulation: From a parts list of regulatory elements to an integrated splicing code. *RNA* 14(5):802–813.
29. Ament SA, et al. (2011) Mechanisms of stable lipid loss in a social insect. *J Exp Biol* 214(Pt 22):3808–3821.
30. Gelfman S, Cohen N, Yearim A, Ast G (2013) DNA-methylation effect on co-transcriptional splicing is dependent on GC-architecture of the exon-intron structure. *Genome Res* 23(5):789–799.
31. Marden JH (2008) Quantitative and evolutionary biology of alternative splicing: How changing the mix of alternative transcripts affects phenotypic plasticity and reaction norms. *Heredity (Edinb)* 100(2):111–120.
32. Merkin J, Russell C, Chen P, Burge CB (2012) Evolutionary dynamics of gene and isoform regulation in Mammalian tissues. *Science* 338(6114):1593–1599.
33. Barbosa-Morais NL, et al. (2012) The evolutionary landscape of alternative splicing in vertebrate species. *Science* 338(6114):1587–1593.
34. Jarosch A, Stolle E, Crewe RM, Moritz RF (2011) Alternative splicing of a single transcription factor drives selfish reproductive behavior in honeybee workers (Apis mellifera). *Proc Natl Acad Sci USA* 108(37):15282–15287.
35. Salz HK (2011) Sex determination in insects: A binary decision based on alternative splicing. *Curr Opin Genet Dev* 21(4):395–400.
36. Bonasio R, et al. (2012) Genome-wide and caste-specific DNA methylomes of the ants Camponotus floridanus and Harpegnathos saltator. *Curr Biol* 22(19):1755–1764.
37. Glastad KM, Hunt BG, Goodisman MA (2013) Evidence of a conserved functional role for DNA methylation in termites. *Insect Mol Biol* 22(2):143–154.
38. Herb BR, et al. (2012) Reversible switching between epigenetic states in honeybee behavioral subcastes. *Nat Neurosci* 15(10):1371–1373.
39. Quinlan AR, Hall IM (2010) BEDTools: A flexible suite of utilities for comparing genomic features. *Bioinformatics* 26(6):841–842.
40. Feng S, Rubbi L, Jacobsen SE, Pellegrini M (2011) Determining DNA methylation profiles using sequencing. *Methods Mol Biol* 733:223–238.

Supporting Information

Li-Byarlay et al. 10.1073/pnas.1310735110

SI Materials and Methods

Image Processing. Treated and control bees were carefully paired. The fluorescent intensity of small interference RNA (siRNA) and nanoparticles (NPs) was measured by Axiovision software via the Measure ⇒ Interactive Measurement ⇒ Start Measurement function. All image data were saved in AxioVision ZVI format. Green channel (NP) and red channel (siRNA) signals were obtained separately and also compared with the background signals to ensure the baseline. A t test was used to assess statistical significance: control ($n = 10$) and *dnmt3* knockdown (KD; $n = 7$). All of the parameters for confocal setting were the same across all samples, including control and treatment bees.

RNA Isolation and Quantitative PCR. RNA was extracted from the fat bodies of each individual bee with the RNeasy kit according to the manufacturer's instructions (Qiagen). Knockdown of *dnmt3* was confirmed by quantitative PCR (qPCR) performed as previously described (1). We selected individuals showing typical KD for RNA sequencing (RNAseq). Primers designed for qPCR experiments and validations of alternative splicing (AS) are listed in Table S4. Sample sizes were 10 treated and 10 control individuals. Primers were designed to cross splice junction-spanning regions of the gene. Genomic DNA was also examined for each primer pair.

RNAseq. Of the 1,190 unexpressed genes, 762 are single-exon genes; only 389 unexpressed genes were annotated in a previous and more conservative annotation OGS v2.0. Read number for each sample is as follows—control sample: 1, 30,689,062 reads (×2); 2, 28,092,866 reads (×2); 3, 27,851,575 reads (×2); 4, 35,186,360 reads (×2); 5, 29,145,865 reads (×2); 6, 28,622,027 reads (×2); *dnmt3* KD sample: 1, 22,658,937 reads (×2); 2, 36,595,658 reads (×2); 3, 29,284,924 reads (×2); 4, 33,208,262 reads (×2); 5, 31,488,264 reads (×2); 6, 34,883,306 reads (×2).

Differential Expression Analysis. TrueSight assigns a probability score to each of the predicted splice junctions for each gene, which indicates their reliability based on coding potentials and RNAseq mapping quality. We used all splice junctions with a TrueSight score >0.5 (on a scale from 0 to 1) to refine the honey bee gene annotation available at the time of this study (Official Gene Set v3.2). A total of 4,274 (5.05% increase) new exons and 20,473 (29.5% increase) new splice junctions were added to OGS v3.2 to improve our analysis. Because the new junctions might originate from AS (alternative exon boundary) and lead to alternative boundaries for a single exon, we extended the original exon boundaries to the most remote junctions on that exon and built a nonredundant exon model for each gene. BEDTools was used to calculate the read coverage of the nonredundant exon models based on TrueSight mapping results (in binary alignment/map format). The sum of read numbers on all exons of a gene represents the digital gene expression value. The SAM (2) permutation test was used to test for differential expression; 2,613 genes (1,357 up-regulated and 1,256 down-regulated) were determined to be differentially expressed [false discovery rate (FDR) = 0.01, $n = 6$ treated and 6 control bees].

Analysis of Alternative Splicing. AS was annotated with the same procedure described in ref. 3. Results for the four subtypes of AS [intron retention (IR), exon skipping (ES), alternative exon boundary (AEB), and alternative terminal exon (ATE)] are summarized in Table 1.

Differential Alternative Splicing. We used two sources of information to test the significance of differentially spliced genes (DSGs). The first approach was to use RNAseq coverage, using both fully mapped reads and junction-spanning reads from RNA-seq; the second approach was to focus on splice junctions, by counting the number of junction-spanning reads from RNA-seq reads on splice junctions involved in AS.

Testing DSG Using Exon/Intron Coverage (P_{cov}). DSGs including IR, ES, and ATE were detected based on the coverage ratio changes for the retaining introns, skipped exons, and alternative terminal exons, respectively. An unpaired t test was used to calculate the P value, P_{cov}, from coverage ratios. Because AEBs often differ by just a few base pairs, exon coverage information cannot be generally applied to AEB differential splicing; only splice junction mapping counts were used to calculate P_{count} (see below).

Testing DSG Using Alternative Splice Junction Mapping Counts (P_{count}). The change in the number of RNA-seq reads mapped onto alternative splice junctions was used to calculate another statistic to test DSG in ES, AEB, and ATE. Fisher's exact test was used to calculate the P value, P_{count}, from alternative splice junction mapping counts. Because IR is for intron expression rather than alternative splice junction, differential IR cannot be tested with junction mappings; only coverage information was used to get P_{cov} (see above).

P_{cov} is the final P value for testing IR and P_{count} is the final P value for testing AEB. For ES and ATE, both statistical testing metrics were applied, and we used Fisher's combined probability test to obtain the final P values: $\chi^2 = -2\log(P_{cov}) - 2\log(P_{count})$. P values were adjusted for multiple hypotheses testing by using a Benjamini-Hochberg FDR criterion. The detailed testing procedure is described below for each subtype of AS.

$$N(x\sim y) = \text{number of reads mapped onto junction } x\sim y$$

$$\text{Cov}(x\sim y) = \frac{\sum_{i=x}^{y}\text{number of reads mapped onto } i}{y-x}.$$

Differential intron retention test. For a retained intron with coordinates $p \sim q$ and two adjacent exons $a \sim p$, $q \sim d$, its inclusion ratio was calculated as follows:

$$\text{IR inclusion ratio} = \frac{2 * Cov(p\sim q)}{Cov(a\sim p) + Cov(q\sim d)}.$$

Unpaired t tests were used on IR inclusion ratios to get P_{cov}, and on that basis, 27 IRs were determined to be DSG (FDR = 0.1; Benjamini-Hochberg). In the example of IR in Fig. 3, control is calculated as $2 \times 40.6/(168.6 + 159.1) \approx 0.25$; *dnmt3* KD is calculated as $2 \times 28.8/(196.1 + 201.9) \approx 0.14$.

Differential exon skipping test. We applied both metrics to measure changes of ES by *dnmt3* KD. For an ES with coordinates $p \sim q$ and two adjacent constitutive exons $a \sim b$, $c \sim d$, the ES skipping ratio was calculated as follows:

$$\text{ES skipping ratio} = \frac{Cov(a\sim b) + Cov(c\sim d) - 2 * Cov(p\sim q)}{Cov(a\sim b) + Cov(c\sim d)}.$$

P_{cov} was calculated using an unpaired t test.

The second method used the number of junction mapping reads. The ES-containing isoform was represented by $I_c = \text{int}\left(\frac{N(b\sim p)+\ N(q\sim c)}{2}\right)$ and the CE-skipping isoform by $I_s = N(b\sim c)$.

For Table 2, we chose 192 differential exon skipping (DES) events together with their flanking 200-bp intronic regions and computed the average change in methylation for each region in *dnmt3* KD vs. control bees. There were 72 DESs overlapping with methylated cytosine-phosphate-guanine (mCpG) sites. Using these 72 DESs, there was a significant relationship between *dnmt3* KD, DNA methylation, and DES; decreased methylation (due to *dnmt3* knockdown) was associated with increased exon skipping (P = 0.019, two-tailed Fisher's exact test). The same analysis was performed for differential intron retention (DIR). Using 15 DIRs, there was also a strong trend with decreased methylation associated with less intron retention (P = 0.044, two-tailed Fisher's exact test).

Although per-sample RNA-seq coverage is decent in our data, minor isoforms generated from AS might still have low sequencing coverage. Therefore, directly comparing the splice junction (SJ) counting ratios across samples would be misleading. We summed all control and *dnmt3* treatment mapping numbers, respectively, performed the Fisher's exact test on the 2 × 2 table $\left[\sum_{i=1}^{6} I_c(i) : \sum_{i=1}^{6} I_s(i);\ \sum_{j=1}^{6} I_c(j) : \sum_{j=1}^{6} I_s(j)\right]$, and calculated P_{count}.

Fisher's combined probability test was performed based on coverage and junction read counts, and the final P value calculated from $\chi^2 = -2\log(P_{cov}) - 2\log(P_{count})$, with four degrees of freedom. A total of 192 ESs were selected as DSGs (0.01 FDR; Benjamini-Hochberg). In the example of ES in Fig. 3, control is calculated as 90/(25 + 46) × 2 ≈ 2.5; *dnmt3* KD is calculated as 197/(40 + 62) × 2 ≈ 3.9.

Differential AEB test. Because the majority of AEBs are of a few base pairs difference, the coverage information could not be applied to differentiate the use of AEBs. Instead, we used RNA-seq read counts on alternative splice junctions in testing differential AEB, as follows.

Let us assume that for three continuous exons ($a \sim b$, $p \sim q$, $c \sim d$), exon $p \sim q$ has alternative splice site p'.

The number of isoforms containing junction $b \sim p$ is $I_p = N(b \sim p)$, and the number of isoforms containing junction $b \sim p'$ is $I_{p'} = N(b \sim p')$. The same Fisher's exact test strategy as used in the differential ES test was applied here in AEB testing.

We determined 141 ATEs to be significantly differentially spliced after *dnmt3* KD, at 0.01 FDR (Benjamini-Hochberg). In the example of AEB in Fig. 3, control is calculated as 121/37 ≈ 3.3; *dnmt3* KD is calculated as 110/10 = 11.

Differential ATE test. Assume that we have a constitutive exon ($a \sim b$), and two ATEs ($c \sim d$, $e \sim f$).

Using the coverage information, ATE splicing ratio was calculated as follows:

$$\text{ATE splicing ratio} = \frac{Cov(c\sim d)}{Cov(c\sim d) + Cov(e\sim f)}.$$

P_{cov} was calculated using an unpaired t test.

The number of isoforms containing junction $b \sim c$ is $I_c = N(b \sim c)$, and the number of isoforms containing junction $b \sim e$ is $I_e = N(b \sim e)$. The same Fisher exact test strategy as used in ES was applied here in ATE testing to calculate P_{count}.

The final P value for ATE was calculated from $\chi^2 = -2\log(P_{cov}) - 2\log(P_{count})$, with four degrees of freedom. In total, 225 ATEs were determined to be DSGs (0.01 FDR; Benjamini-Hochberg). In the example of ATE in Fig. 3, control is calculated as 87/27 ≈ 3.2; *dnmt3* KD is calculated as 179/34 ≈ 5.3.

1. Alaux C, et al. (2009) Honey bee aggression supports a link between gene regulation and behavioral evolution. *Proc Natl Acad Sci USA* 106(36):15400–15405.
2. Li J, Tibshirani R (2011) Finding consistent patterns: A nonparametric approach for identifying differential expression in RNA-Seq data. *Stat Methods Med Res*, 10.1177/0962280211428386.
3. Li Y, et al. (2013) TrueSight: A new algorithm for splice junction detection using RNAseq. *Nucleic Acids Res* 41(4):e51.

ATGTTGTCCGAGGAAGGGAAATTATGGGTTTACTGGATCGGAGAAGCTCGTATATCATTA
TTGAACGAAAAGACGCAGATCGAACCGTTCTCGTGTAACCTCAAGGCTAGACTGACGCAG
AATTTAAACGTACCGCGAATTCGTGCCATTGACGCAACTATGCAGATGTTGCGCAAAAAA
TTGGGCGGTACTTTGACCAAGCCGTATTTCACGTGGATCGAAAGCAATTTCCCCAAAAAT
ATGATCGAAATGTTGGACGAAATCAAGTTTTATCCGTATCCGGTAAAGATGCAACAAAGA
TTGGACCATCTTAGGGAAAAAAAACGCAAAAGTAACGGAAAGATATTTATTGGATCAAAAA
CGGGAAAATCAAGAGAAAAAATTGGCTGAGAAGTCGAAAGATTCGCCGCAAAAAGTCAAC
GTAGATTTGACGCTTTTGCCGTTGAAAGAGCAGAAACCGGGAATTATAGCCTGGGCTAAA
ATTGCCGGGCACAATTGGTGGCCAGCGATGATTATCGATTATCGCGACTGTTGCATGCGA
GAACCGACGTTCGGTTGCCAATGGATCATGTGGTACGGCGACTACAAACTGTCGGAGGTG
CATCATCAATTGTTCTTGAGGTTCGACAAGGGGATGGAGAAAATGCGCGACTACACGAGC
AACACGAAGAAGCATATCTACCTCGTAGGAGTTCTCCAAGCCTCCAAGGATTATTGCTCC
CGTCTAGGATTCGATACCTCCAACTGGACTTTGGACGACGCTTTCGAATATTTTTCCAAG
CCTAATCATTACGATTACGCGTCGTCTGCGAACACTTGGAGGAGAGAAGACTCGGTCAAG
ATCTACGACAAGTACTCGGCCCGCATCGCGGAAAAATTGAACGAGCTGAAGGACAATCCG
AACGTGGACGACCAACGGGCCAACGATATAAACAACAGCGATGACCTGCGATCGGCGATA
AAAGGGGAAATCTCGTTCGACTCGTTGTGCCTCAAGTGCCTTCGAGTTTCCAACGACGAA
ATGGACATTCATCCGTTCTTCGAGGGATCTTTGTGCAAAGATTGTTCGGAACGATATAAA
CCCTGTATGTTCGTTTTCGGTAACGACTCCAAATGCTTTTATTGCACCGTGTGCGCCGCC
TCTGGGATGGTGATCATCTGCGACAAAGAAGATTGTCCAAGGGTTTACTGCACCGCCTGC
ATGAAACACCTCCTGTGCCCGACGACTTACGAGCAAGTGCTCCAGGAGGATCCTTGGGAA
TGCTTCCTCTGCAAGTCAAGATCTTTCACCACAGACACCATCGTCAGGCCTCGAGCTAAT
TGGAAGGACAAGATAATCAATATGTTCCGTACCAGTTGCGACTCGAATGTGGAACACCTG
GTTGCCAAGCATAATTCAGAGAAGAGAAAAATACGCGTTCTCTCCCTGTTCGACGGCCTT
GGCACAGGTTTGCTCGTACTTCTGAAACTGGGCTTCATCGTGGACGCGTATTACGCGAGC
GAGATAGACCAAGACGCGTTGATGGTTACCGCCTCGCACTTCGGCGACCGTATCCTCCAA
TTGGGCAACGTGAAGGACATCACGTGTAACACGATCAAAGAGATAGCTCCCATCGATCTT
CTGATCGGTGGATCGCCGTGCAACGATCTCAGCTTGGCCAATCCTGCCCGCCTCGGCCTC
CACGATCCCAGAGGAACGGGTGTACTGTTCTTCGAGTACCGTCGAATTCTGAAACTGGTG
AGGAAGCTTAATAACGAGCGGCATTTGTTCTGGTTGTACGAGAACGTCGCCTCGATGCCC
AGCGAGTACAGATTGGAGATCAACAAACATCTAGGACAGGAACCGGACGTGATAGACTCG
GCAGACTTCTCGCCCCAGCACAGATTGAGACTGTACTGGCACAACTTTCCCATAGAGCCA
CGTCTGTTATCGTCCCAAAGGGAGCAGGACGTGCAGGATATACTTACGCCGCATTGCCAA
CGTTACTCGTTGGTCAAAAAGATACGCACAGTCACTACGAAAGTGAACTCGTTGAAGCAA
GGTGATGGCAAACTTGCGTTGAAACCAATTTTGATGAAGGACGAAAGCGACTCGTTGTGG
ATAACAGAGCTGGAGGAAATATTCGGGTTCCCGCGTCATTACACGGACGTAAAGAATTTA
TCTGCGACGAAAAGGCAGAGGTTAATAGGTAAATCTTGGAGCGTGCAAACGTTGACAGCC
ATTTTCGAATCTCTTTGTCCCTTTTTCGAGCGCGATATCGTGGAAATCGAGGGATGA

Fig. S1. mRNA sequence of *dnmt3* (GB55485) and KD sites. The italicized and gray colored sequences are the siRNA target sites (exon 5, location starts at 413; ref. 1). The underlined and yellow colored sequences are the qPCR primers (exon 12, location of forward primer starts at 1,211, and reverse primer at 1,273).

1. Kucharski R, Maleszka J, Foret S, Maleszka R (2008) Nutritional control of reproductive status in honeybees via DNA methylation. *Science* 319(5871):1827–1830.

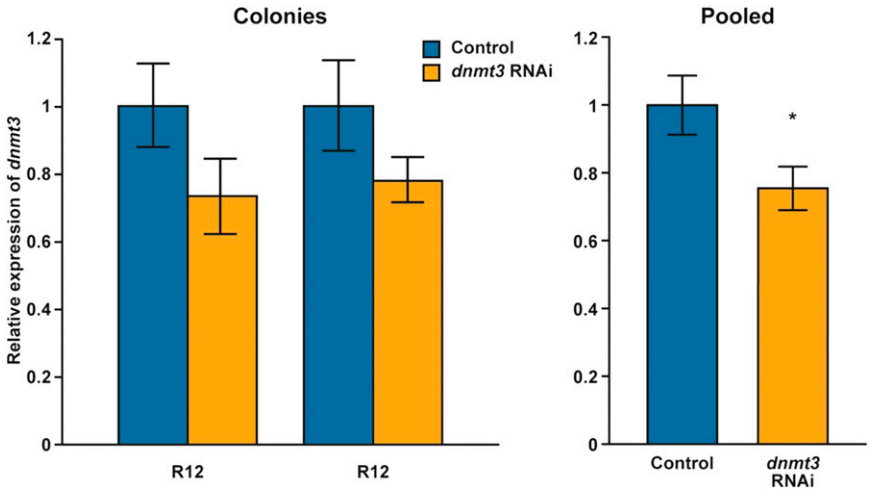

Fig. S2. KD effects on *dnmt3* mRNA expression by injecting *dnmt3* siRNA in the abdomen of honey bees (mean and SEM). Shown are two biological replicates ($n = 21$ and 22, P values based on two-tailed t-tests) and results from pooled data (mixed-model ANOVA, df = 40, $F = 6.18$, $^*P < 0.05$).

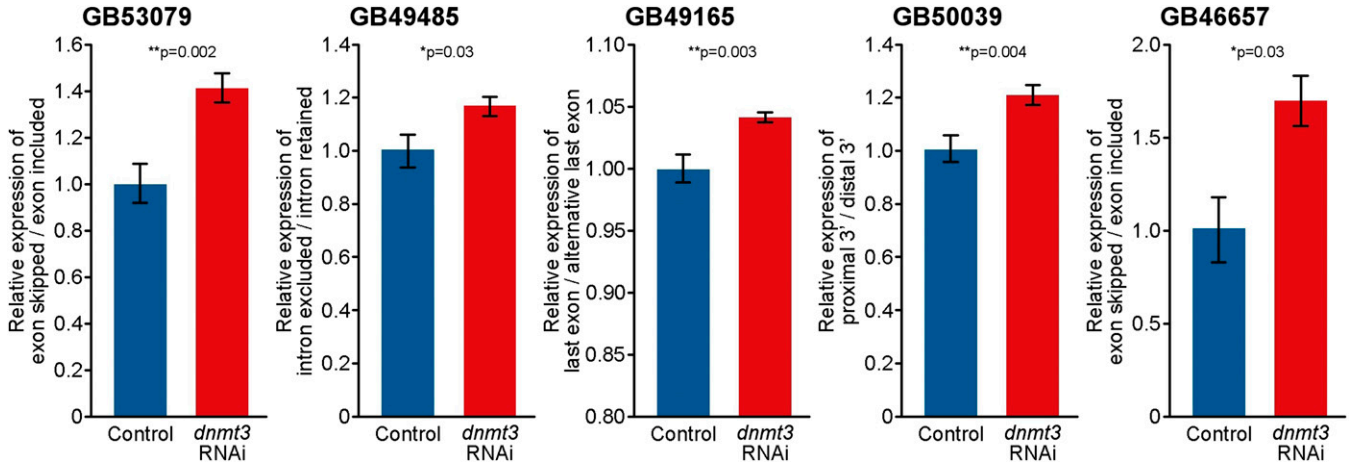

Fig. S3. Validation of *dnmt3* RNAi-associated alternative splicing. To validate the splicing results, gene candidates for each type of AS event were selected for qPCR analysis. ES was validated with *GB53079* (motile sperm domain-containing protein 1-like) and *GB46657* (galactokinase-like); IR with *GB49485* (probable prolyl-tRNA synthetase, mitochondrial-like); ATE with gene *GB49165* (protein RER1-like); and AEB with gene *GB50039* (methionyl-tRNA synthetase). Control: $n \geq 10$; *dnmt3* KD: $n \geq 10$. Mean relative expression levels, SEM, and *P* values are displayed. Data analyzed with two-tailed *t* tests.

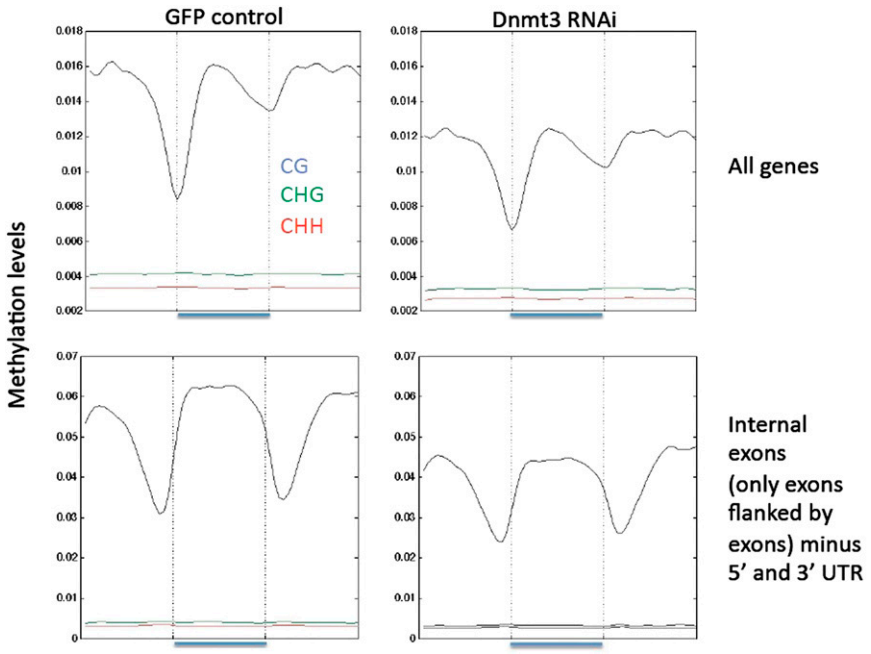

Fig. S4. Methylation levels for control and *dnmt3* KD bees ($n = 1$ pooled sample for each). Top two graphs show all genes; bottom two graphs show internal exons only. C stands for cytosine, G stands for guanine, H stands for adenine (A), thymine (T), or cytosine (C). The colors blue, green, and red represent CG, CHG, and CHH sequences, respectively. The middle section (underlined blue) of each graph represents the whole gene or just the internal exon.

Table S1. Gene Ontology (biological process) analysis of genes that were differentially expressed between control bees and *dnmt3* KD bees (Benjamini cutoff: <0.01)

Term	Count	Percentage	*P* value	Fold enrichment	Benjamini
GO:0042254~ribosome biogenesis	44	2.31	2.91E−20	4.32	7.21E−17
GO:0022613~ribonucleoprotein complex biogenesis	51	2.68	4.23E−17	3.41	5.24E−14
GO:0034660~ncRNA metabolic process	61	3.21	9.67E−16	2.88	8.25E−13
GO:0006396~RNA processing	102	5.36	1.25E−13	2.06	7.74E−11
GO:0034470~ncRNA processing	43	2.26	1.27E−11	2.94	6.30E−09
GO:0006364~rRNA processing	25	1.31	2.60E−10	3.93	1.07E−07
GO:0006413~translational initiation	30	1.58	2.65E−10	3.43	9.37E−08
GO:0016072~rRNA metabolic process	25	1.31	5.33E−10	3.83	1.65E−07
GO:0046907~intracellular transport	90	4.73	7.16E−09	1.81	1.97E−06
GO:0030163~protein catabolic process	65	3.42	7.51E−09	2.04	1.86E−06
GO:0019941~modification-dependent protein catabolic process	57	3.00	1.66E−08	2.12	3.75E−06
GO:0043632~modification-dependent macromolecule catabolic process	57	3.00	2.11E−08	2.11	4.35E−06
GO:0044257~cellular protein catabolic process	60	3.15	2.15E−08	2.06	4.09E−06
GO:0051603~proteolysis involved in cellular protein catabolic process	60	3.15	2.15E−08	2.06	4.09E−06
GO:0034621~cellular macromolecular complex subunit organization	64	3.36	3.65E−08	1.98	6.45E−06
GO:0034622~cellular macromolecular complex assembly	55	2.89	4.84E−08	2.10	7.99E−06
GO:0043933~macromolecular complex subunit organization	80	4.21	8.81E−08	1.79	1.36E−05
GO:0006399~tRNA metabolic process	37	1.95	1.08E−07	2.48	1.57E−05
GO:0065003~macromolecular complex assembly	72	3.79	1.31E−07	1.84	1.81E−05
GO:0044265~cellular macromolecule catabolic process	67	3.52	1.89E−07	1.87	2.47E−05
GO:0007010~cytoskeleton organization	116	6.10	2.50E−07	1.57	3.10E−05
GO:0045184~establishment of protein localization	79	4.15	3.59E−07	1.74	4.23E−05
GO:0015031~protein transport	77	4.05	5.33E−07	1.74	6.00E−05
GO:0008104~protein localization	100	5.26	6.45E−07	1.60	6.95E−05
GO:0009057~macromolecule catabolic process	76	4.00	9.53E−07	1.73	9.83E−05
GO:0007017~microtubule-based process	102	5.36	1.06E−06	1.58	1.05E−04
GO:0051169~nuclear transport	29	1.52	1.95E−06	2.53	1.86E−04
GO:0006913~nucleocytoplasmic transport	29	1.52	1.95E−06	2.53	1.86E−04
GO:0006457~protein folding	39	2.05	3.61E−06	2.13	3.31E−04
GO:0060341~regulation of cellular localization	27	1.42	6.51E−06	2.50	5.75E−04
GO:0000226~microtubule cytoskeleton organization	77	4.05	9.17E−06	1.63	7.83E−04
GO:0006886~intracellular protein transport	51	2.68	1.09E−05	1.84	8.99E−04
GO:0034613~cellular protein localization	52	2.73	1.16E−05	1.83	9.25E−04
GO:0016192~vesicle-mediated transport	95	4.99	1.17E−05	1.53	9.05E−04
GO:0006605~protein targeting	36	1.89	1.76E−05	2.08	1.32E−03
GO:0006325~chromatin organization	49	2.58	2.70E−05	1.81	1.96E−03
GO:0016568~chromatin modification	36	1.89	3.37E−05	2.02	2.38E−03
GO:0007051~spindle organization	60	3.15	3.88E−05	1.68	2.66E−03
GO:0006612~protein targeting to membrane	15	0.79	4.45E−05	3.25	2.98E−03
GO:0007052~mitotic spindle organization	53	2.79	5.93E−05	1.72	3.86E−03
GO:0044087~regulation of cellular component biogenesis	28	1.47	5.99E−05	2.20	3.80E−03
GO:0016044~membrane organization	78	4.10	6.32E−05	1.54	3.90E−03
GO:0007242~intracellular signaling cascade	73	3.84	9.41E−05	1.55	5.67E−03
GO:0009451~RNA modification	17	0.89	1.02E−04	2.81	6.01E−03
GO:0000022~mitotic spindle elongation	27	1.42	1.03E−04	2.18	5.93E−03
GO:0006897~endocytosis	65	3.42	1.13E−04	1.58	6.33E−03
GO:0010324~membrane invagination	65	3.42	1.13E−04	1.58	6.33E−03
GO:0006338~chromatin remodeling	19	1.00	1.20E−04	2.60	6.59E−03
GO:0043623~cellular protein complex assembly	28	1.47	1.22E−04	2.12	6.57E−03
GO:0070727~cellular macromolecule localization	62	3.26	1.28E−04	1.60	6.75E−03
GO:0051231~spindle elongation	27	1.42	1.31E−04	2.15	6.74E−03
GO:0006461~protein complex assembly	46	2.42	1.60E−04	1.73	8.06E−03
GO:0070271~protein complex biogenesis	46	2.42	1.60E−04	1.73	8.06E−03
GO:0007317~regulation of pole plasm oskar mRNA localization	13	0.68	1.69E−04	3.27	8.33E−03
GO:0006909~phagocytosis	52	2.73	1.81E−04	1.66	8.73E−03

Table S2. Effects of *dnmt3* KD on expression and methylation of genes known to encode splicing factors (based on orthology to *Drosophila melanogaster*)

OGS3.2 Gene name	Up-regulated (Q value)	Down-regulated (Q value)	Fold change	Fold change: gene body methylation	Fold change: promoter	Fly ortholog	Gene function
GB51710		0.61	0.81	1.22	0.49	FBgn0001942	Eukaryotic initiation factor 4A-like
GB50757		0.53	0.85	0.66	0.71	FBgn0022987	KH domain-containing, RNA-binding, signal transduction-associated protein 3–like [*Apis mellifera*]
GB55439		0.49	0.89	1.04	0.00	FBgn0010220	DEAD box protein 45A ortholog
GB42714	0.68		1.11	0.99	0.63	FBgn0086683	Splicing factor 45-like
GB49296	0.85		1.11	0.80	1.96	FBgn0030974	U2AF_lg; U2 snRNP auxilliary factor, large subunit, splicing factor
GB48312	0.25		1.13	0.99	0.94	FBgn0037220	Pre-mRNA-splicing factor RBM22-like
GB48261	0.06		1.15			FBpp0084626	116-kDa U5 small nuclear ribonucleoprotein component–like
GB50695	0.56		1.17	0.98	0.98	FBgn0086444	Probable pre-mRNA-splicing factor ATP-dependent RNA helicase mog-4–like
GB44439	0.09		1.18	1.10	1.13	FBgn0037573	Eukaryotic initiation factor 4A-III–like
GB50078	0.62		1.20	0.67	0.75	FBgn0015331	ATP-dependent RNA helicase activity
GB51256	0.09		1.25	0.53	0.98	FBgn0036314	PRP11; Splicing factor 3a, subunit 2 [RNA processing and modification]
GB42720	0.09		1.36	1.12	1.29	FBgn0014189	Helicase at 25E ortholog
GB42279	0.21		1.38	0.97	0.00	Null	DEADc; DEAD-box helicases; a diverse family of proteins involved in ATP-dependent RNA unwinding, needed in a variety of cellular processes including splicing, ribosome biogenesis and RNA degradation
GB40538	0.09		1.67	1.40	0.91	FBgn0021995	Probable ATP-dependent RNA helicase DDX27-like
GB50605	0.09		1.70	0.76	0.00	FBgn0038609	Putative pre-mRNA–splicing factor ATP-dependent RNA helicase DHX15-like
GB44884	0.21		1.89	0.98	1.59	FBgn0035162	Splicing factor 3b, subunit 3, 130 kDa

Gene list obtained from the National Center for Biotechnology Information (NCBI) database.

Table S3. siRNA sequence designed for RNA interference (ref. 1)

siRNA	Sense	Antisense
EGFP-S1 DS positive control duplex	ACCCUGAAGUUCAUCUGCACCACCG	CGGUGCAGAUGAACUUCAGCCUCA
dnmt3	GUCAACGUAGAUUUGACGCdTdT	GCGUCAAAUCUACGUUGACdTdT

1. Kucharski R, Maleszka J, Foret S, Maleszka R (2008) Nutritional control of reproductive status in honeybees via DNA methylation. *Science* 319(5871):1827–1830.

Table S4. Primers used for qPCR experiments

Primer names	Forward	Reverse
Eif3-S8	TGA GTG TCT GCT ATG GAT TGC AA	TCG CGG CTC GTG GTA AA
GAPDH	ACT GGT ATG GCC TTC CGT GTA C	TGC CAA GTC TAA CTG TTA AGT CAA CA
dnmt3	TCC TGT GCC CGA CGA CTT A	TGC AGA GGA AGC ATT CCC A
GB53079 exon included	GTC CAG CTA TAC AAA TGA TTC CAG C	ATG CTA TGG ATA AAG GAG GAA CAA A
GB53079 exon skipped	GTC CAG CTA TAC AAA TGA TTC CAG C	CAA AAT AAA GCA ATT GAT AGA GGA ACA A
GB50039 ctrl-186–495	TCT TCC TGT TTT TCT TTT TTT TTT TGT AAC	TTT ACA ACG TGT CAA AAA TCA AGA GA
GB50039 -178–495	AAA TGT GAT TTT GCT TCA CTT TGA TAA A	ACG TGT CAA AAA TCA AGA GAA GTT ACA A
GB49165 -9476082–2735	TTC CTT AGG TTA GCG CCA AGA T	CTC ATG GAA AAC CAA AGT ACC AGA
GB49165 -9480053–2735	CCA TCA CCA AAT TTC CAC GG	CTC ATG GAA AAC CAA AGT ACC AGA
GB53833 -9158642–8319	TGA ACA TCA AGA CGA AGT GGA TG	CGT CTA TAC GCT TGG TCA GCC T
GB53833 -9191360–8319	AAA TCA AGA GCA TCG TGA TCG AG	CGT CTA TAC GCT TGG TCA GCC T
GB49485 E1	TGG CCA AAA AAT TTA GCA CCA	TTT TCT TCT TTG CTT CCT GCC T
GB49485 E2	GAA GAA TTA AGA TGG CCA AAA AAT TTA	ATA CCC TTT TAT ATA TTA CCT TTG GTG GT
GB46657 exon included	TCG TGT GAA TTT AAT CGG AGA ACA	GTA ACC ATG GGC AAT GCC A
GB46657 exon skipped	TGT ATG TGC ACC CGG TCG	GCA TTA AAA GGT GGC ACA TCA C